JACS
JOURNAL OF THE AMERICAN CHEMICAL SOCIETY
Article
pubs.acs.org/JACS

# CO Oxidation Catalyzed by Single Gold Atoms Supported on Aluminum Oxide Clusters

Zi-Yu Li,[†,‡] Zhen Yuan,[†,‡] Xiao-Na Li,*[,†] Yan-Xia Zhao,[†] and Sheng-Gui He*[,†]

[†]Beijing National Laboratory for Molecular Sciences, State Key Laboratory for Structural Chemistry of Unstable and Stable Species, Institute of Chemistry, Chinese Academy of Sciences, Beijing 100190, People's Republic of China

[‡]University of Chinese Academy of Sciences, Beijing 100049, People's Republic of China

Supporting Information

**ABSTRACT:** The single gold atom doped aluminum oxide clusters $AuAl_3O_3^+$, $AuAl_3O_4^+$, and $AuAl_3O_5^+$ have been prepared and mass-selected to react with CO, $O_2$, and mixtures of CO and $O_2$ in an ion trap reactor under thermal collision conditions. The reactions have been characterized by mass spectrometry with isotopic substitution ($^{16}O_2 \rightarrow {}^{18}O_2$) and density functional theory calculations. The $AuAl_3O_5^+$ cluster can oxidize two CO molecules consecutively to form $AuAl_3O_4^+$ and then $AuAl_3O_3^+$, the latter of which can react with one $O_2$ molecule to regenerate $AuAl_3O_5^+$. The $AuAl_3{}^{16}O_3^+$ ions interact with a mixture of $C^{16}O$ and $^{18}O_2$ to produce the fully substituted $^{18}O$ species $AuAl_3{}^{18}O_{3-5}^+$, which firmly identifies a catalytic cycle for CO oxidation by $O_2$. The oxidation catalysis is driven by electron cycling primarily through making and breaking a gold−aluminum chemical bond. To the best of our knowledge, this is the first identification of catalytic CO oxidation by $O_2$ mediated with gas-phase cluster catalysts with single-noble-metal atoms, which serves as an important step to understand single-atom catalysis at strictly a molecular level.

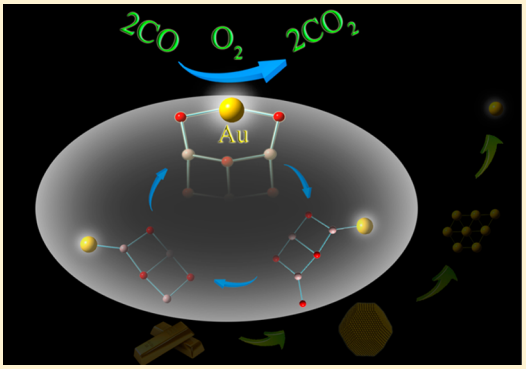


## 1. INTRODUCTION

Recently, there has been an increasing interest in developing single-atom catalysts with isolated noble metal (NM) atoms dispersed on solid supports in order to maximize the effective use of the precious metals and offer great potential for achieving high chemical activity and selectivity.[1] Many supported NM atoms, including Au, Pt, Ir, Rh, and Pd, have been demonstrated to catalyze important reactions such as the oxidation of carbon monoxide ($2CO + O_2 \rightarrow 2CO_2$),[2] water-gas shift ($CO + H_2O \rightarrow CO_2 + H_2$),[3] hydrogenation of unsaturated compounds (e.g., $C_4H_6 + H_2 \rightarrow C_4H_8$),[4] and so on.[1] It is of great importance to understand the mechanisms of single-atom catalysis at a molecular level for the rational design of better-performing catalysts. However, it is technically very difficult to characterize the chemical bonding and reactivity involved with individually supported metal atoms in condensed-phase systems. For example, scanning transmission electron microscopy (STEM) with subangstrom spatial resolution identified five different Pt atom adsorption sites on a clean $TiO_2$ (110) surface, while the experimental characterization of the catalytic activity for each Pt site can be extremely challenging.[5] Therefore, it is very important to adopt an alternative method to study the detailed structure−property relationships in single-atom catalysis.

It has long been proposed that gas-phase atomic clusters that can be well characterized by both experimental and computational methods are the ultimate single-site catalysts.[6] Herein, we demonstrate that, by doping single gold atoms into aluminum oxide clusters, it is possible to understand a rather detailed mechanism of single gold atom catalysis in the oxidation of carbon monoxide by molecular oxygen. The oxidation of CO into $CO_2$ serves as an important process in air purification and a prototypical reaction for heterogeneous catalysis. Supported gold nanoparticles and clusters are well-known to catalyze CO oxidation.[7] Well-controlled experiments indicated that $Au_8$ on MgO (001) is the smallest active gold cluster[8] and $Au_{1,2}$ on $TiO_2$ species are almost inert in catalytic CO oxidation.[9] Studies of gas-phase cluster systems identified that the gold dimer ($Au_2^-$) rather than the monomer is the smallest naked gold species catalyzing CO oxidation.[10] These gold cluster investigations are in sharp contrast to very recent experiments with the imaging of aberration-corrected STEM that atomically dispersed gold in a zeolite is active for catalytic CO oxidation.[11] It is interesting to study how and why a single gold atom can be catalytic, which is also very important for the rational design of single-Au catalysts.

## 2. METHODS

**2.1. Experimental Methods.** The $AuAl_xO_y^+$ clusters were generated by laser ablation of a mixed-metal disk compressed with Au and Al powders (molar ratio Au/Al = 10/1) in the presence of 0.15% $O_2$ seeded in a He carrier gas with a backing pressure of 6.5 standard atmospheres. The $AgAl_xO_y^+$ clusters were also generated in a

Received: August 20, 2014
Published: September 12, 2014

   dx.doi.org/10.1021/ja508547z | J. Am. Chem. Soc. 2014, 136, 14307−14313

similar way (molar ratio Ag/Al = 1/2) for comparative studies. The cluster ions of interest were mass-selected by a quadrupole mass filter (QMF) and then entered into a linear ion trap (LIT) reactor, where they were thermalized by collisions with a pulse of He gas and then interacted with a pulse of CO, $O_2$, or a mixture of $CO/O_2$ for around 1.0 ms. The instantaneous gas pressure of He in the reactor was around 2−4 Pa, and the partial pressures of the reactant molecules ranged from about 1 mPa to more than 100 mPa, depending on the reaction systems. The assessment of thermalization for the cluster ions before the interactions with reactant gas molecules in the LIT reactor can be found in previous studies.[12] The temperature of the cooling gas (He), the reactant gases (CO, $O_2$, and a mixture of CO and $O_2$), and the LIT reactor was around 298 K. The cluster ions ejected from the LIT were detected by a reflectron time-of-flight mass spectrometer (TOF-MS). The details of running the TOF-MS,[13] the QMF,[14] and the LIT[12a] can be found in our previous works.

Assuming a pseudo-first-order reaction mechanism, the ion intensity ($I_i$) of the $i$th cluster at time $t$ in the reactor generally follows the equation array ($i$ = 1, 2, 3, ..., $N$ and $N \geq 2$)

$$\frac{dI_i}{dt} = \sum_{j \neq i} k_{j \rightarrow i} n_j I_j - \left(\sum_{k \neq i} k_{i \rightarrow k} m_k\right) I_i \quad (1)$$

in which $n_j$ is the density of the $j$th gas molecules that can react with the $j$th cluster with the pseudo-first-order rate constant of $k_{j \rightarrow i}$ to convert the $j$th cluster to the $i$th cluster (cluster $j$ + gas $j$ with density $n_j$ $\xrightarrow{k_{j \rightarrow i}}$ cluster $i$) and $m_k$ is the density of the $k$th gas molecules that can react with the $i$th cluster with the pseudo-first-order rate constant of $k_{i \rightarrow k}$ to convert the $i$th cluster to the $k$th cluster (cluster $i$ + gas $k$ with density $m_k$ $\xrightarrow{k_{j \rightarrow i}}$ cluster $k$). To determine the rate constants $k_{j \rightarrow i}$ and $k_{i \rightarrow k}$, the ion intensities ($I_i$) at a fixed reaction time $t = t_R$ and variable reactant gas pressures (or densities, $n_j$ and $m_j$) were recorded. It is noteworthy that in our experiments with the pulsed cooling (He) and reactant gases, the instantaneous gas pressures during the short reaction time ($t_R \approx 1.0$ ms) can be almost constant; thus, the reaction time was fixed and the reactant gas pressures were varied.[12a] A Fortran code was developed to solve the equation array (1) numerically so that the ion intensities $I_i$ at $t = t_R$ could be calculated under given values of reactant gas pressures and rate constants. The calculated $I_i$ values were least-squares fitted to the experimental ion intensities in order to determine the experimental rate constants (Figures S2−S6 in the Supporting Information). To calculate reaction efficiencies (the possibilities of reaction upon each collision), the collision rate constants were calculated on the basis of the surface charge capture model developed in literature.[15]

**2.2. Theoretical Methods.** Density functional theory (DFT) calculations using Gaussian 09 program[16] were carried out to investigate the structures of the Au−Al−O and Ag−Al−O clusters as well as the mechanisms of the Au−Al−O cluster reactions with CO and $O_2$ molecules. In order to find an appropriate functional, the bond dissociation energies of Au−Al, Au−O, Ag−Al, Ag−O, Al−O, C−O, and O−O were computed by various functionals and compared with available experimental data (Table S1 in the Supporting Information). It turns out that with the TZVP basis sets[17] for Al, C, and O atoms and a D95V basis set[18] combined with the Stuttgart/Dresden relativistic effective core potential (denoted as SDD in Gaussian software) for Au and Ag atoms, the TPSS functional,[19] was the best overall; thus, the results by TPSS are given throughout this work. A Fortran code based on genetic algorithm was used to generate initial guess structures of the clusters.[20] The reaction mechanisms were studied for $AuAl_3O_{4,5}^+$ + CO and $AuAl_3O_{3,4}^+$ + $O_2$ systems. This involved geometry optimizations of reaction intermediates (IMs) and transition states (TSs) through which the IMs transfer to each other. The initial guess structures of the TS species were obtained through relaxed potential energy surface scans using single or multiple internal coordinates.[21] Vibrational frequency calculations were performed to check that the IMs or TSs have zero and only one imaginary frequency, respectively. Intrinsic reaction coordinate calculations were performed so that a transition state connects two appropriate local minima. The zero-point vibration corrected energies ($\Delta H_0$) in units of eV are reported in this work. Natural bond orbital (NBO) analysis was performed with NBO 3.1.[22]

## 3. RESULTS

**3.1. Experimental Results.** Each of the $AuAl_3O_3^+$, $AuAl_3O_4^+$, and $AuAl_3O_5^+$ clusters was mass-selected and interacted with CO and $O_2$ molecules in the ion trap reactor separately. The $AuAl_3O_3^+$ cluster (Figure 1a) is inert with CO

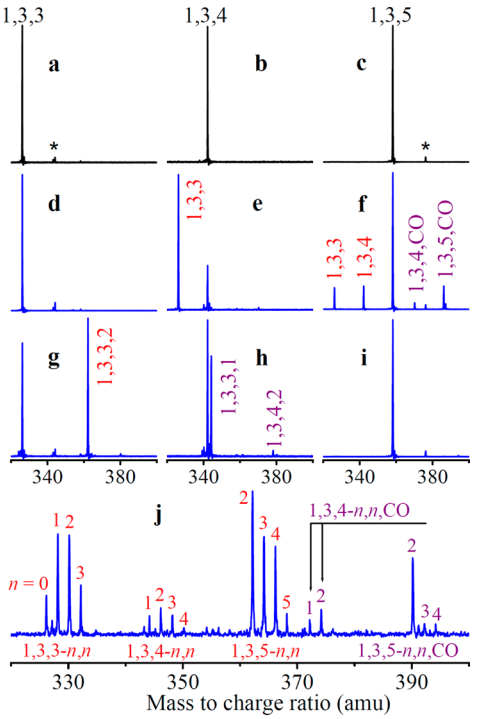


**Figure 1.** Elementary and catalytic reactions of the atomic cluster ions. Mass spectra for elementary reactions of mass-selected $AuAl_3{}^{16}O_{3-5}^+$ (a−c) with $C^{16}O$ and $^{18}O_2$ are shown in panels d−f and g−i, respectively. The CO partial pressures were 7 mPa (d), 6 mPa (e), and 6 mPa (f). The $^{18}O_2$ partial pressures were 7 mPa (g), 8 mPa (h), and 20 mPa (i). Panel j shows the mass spectrum for reactions of $AuAl_3{}^{16}O_3^+$ with a gas mixture of 66 mPa of $C^{16}O$ and 33 mPa of $^{18}O_2$. The time periods for all of the reactions were 1.0 ms. The $Au_xAl_y{}^{16}O_z^+$ and $Au_xAl_y{}^{16}O_zCO^+$ species are labeled as $x,y,z$ and $x,y,z$,CO, respectively. Similarly, $Au_xAl_y{}^{16}O_{z-n}{}^{18}O_n^+$ ($n \neq 0$) is labeled as $x,y,z$-$n,n$, and $Au_xAl_y{}^{16}O_{z-n}{}^{18}O_nCO^+$ is labeled as $x,y,z$-$n,n$,CO. Peaks marked with asterisks are due to water impurities. See also Figures S1 and S8 in the Supporting Information for more information.

(Figure 1d) but can pick up an $O_2$ molecule to generate $AuAl_3O_5^+$ (Figure 1g). The opposite reactivity was observed for $AuAl_3O_5^+$ (Figure 1c), which is inert with $O_2$ (Figure 1i) but can react with CO to generate the product clusters $AuAl_3O_{3,4}^+$ and $AuAl_3O_{4,5}CO^+$ (Figure 1f). The $AuAl_3O_4^+$ cluster (Figure 1b) is reactive with both CO (Figure 1e) and $^{18}O_2$ (Figure 1h) to generate $AuAl_3O_3^+$ and $AuAl_3{}^{16}O_3{}^{18}O^+$, respectively. Pressure-dependent experiments indicated that the formations of $AuAl_3O_3^+$ and $AuAl_3O_4CO^+$ shown in Figure 1f are due to secondary reactions. The primary reactions observed are

$$AuAl_3O_5^+ + CO \rightarrow AuAl_3O_4^+ + CO_2 \quad (2a)$$

$$AuAl_3O_5^+ + CO \rightarrow AuAl_3O_5CO^+ \quad (2b)$$


dx.doi.org/10.1021/ja508547z | J. Am. Chem. Soc. 2014, 136, 14307−14313

$$AuAl_3O_4^+ + CO \rightarrow AuAl_3O_3^+ + CO_2 \quad (3a)$$

$$AuAl_3{}^{16}O_4^+ + {}^{18}O_2 \rightarrow AuAl_3{}^{16}O_3{}^{18}O^+ + {}^{16}O^{18}O \quad (3b)$$

$$AuAl_3O_3^+ + O_2 \rightarrow AuAl_3O_5^+ \quad (4)$$

The pseudo-first-order rate constants for the above reactions can be well fitted (Figures S2−S5 in the Supporting Information), and some of the results are given in the second column of Table 1. The reaction efficiencies are 11%, 83%, and 42% for reactions 2a, 3a, and 4, respectively.

**Table 1. Pseudo-First-Order Rate Constants Determined from Elementary and Catalytic Reactions**[a]

| | elementary | catalytic |
|---|---|---|
| $AuAl_3O_5^+ + CO \rightarrow AuAl_3O_4^+ + CO_2$ | 1.5 | 2.8 |
| $AuAl_3O_4^+ + CO \rightarrow AuAl_3O_3^+ + CO_2$ | 11 | 7.3 |
| $AuAl_3O_3^+ + O_2 \rightarrow AuAl_3O_5^+$ | 4.6 | 3.3 |

[a]The values are in unit of $10^{-10}$ $cm^3$ $molecule^{-1}$ $s^{-1}$. The uncertainties of the absolute and relative rate constants are within ±40% and ±20%, respectively.

The elementary reactions (2a), (3a), and (4) comprise a catalytic cycle for CO oxidation by $O_2$ mediated with the $AuAl_3O_{3-5}^+$ clusters (Figure 2a and eq 5):

$$2CO + O_2 \xrightarrow{AuAl_3O_{3-5}^+ \text{ catalysts}} 2CO_2 \quad (5)$$

To confirm that the catalytic cycling is really happening, for example, the $AuAl_3O_5^+$ cluster produced from reaction 4 can oxidize a CO molecule to generate $AuAl_3O_4^+$ (reaction 2a), such formed $AuAl_3O_4^+$ can oxidize a second CO (reaction 3a), and so forth, each of the $AuAl_3{}^{16}O_{3-5}^+$ clusters was mass-selected and interacted with mixtures of $C^{16}O$ and $^{18}O_2$. This indicated that the cycling really takes place starting from any of the species $AuAl_3{}^{16}O_3^+$ (Figure 1j and Figures S7 and S8 in the Supporting Information), $AuAl_3{}^{16}O_4^+$ (Figure S9 in the Supporting Information), and $AuAl_3{}^{16}O_5^+$ (Figure S10 in the Supporting Information). Figure 1j indicates that, starting from $AuAl_3{}^{16}O_3^+$, the $^{16}O$ atoms in this cluster can be substituted by isotopic $^{18}O$ to generate $AuAl_3{}^{16}O_2{}^{18}O^+$, $AuAl_3{}^{16}O{}^{18}O_2^+$, and $AuAl_3{}^{18}O_3^+$. These $^{18}O$ species must be generated from the catalytic cycle (Figure 2a) because the $^{16}O/^{18}O$ exchange reaction does not take place in the reaction of $AuAl_3{}^{16}O_3^+$ with $^{18}O_2$ (Figure 1g). Similarly, generations of $AuAl_3{}^{16}O_{5-n}{}^{18}O_n^+$ ($n$ = 2−5) and $AuAl_3{}^{16}O_{4-n}{}^{18}O_n^+$ ($n$ = 1−4) further confirm the catalysis. Minor reaction channels due to the adsorptions of $H_2O$ impurity and CO reactant molecules were also observed, particularly under the conditions of relatively high CO partial pressures (Figures S7 and S8). These processes correspond to catalyst deactivation such as catalyst poisoning by CO[23] usually presented in model and practical catalysis.

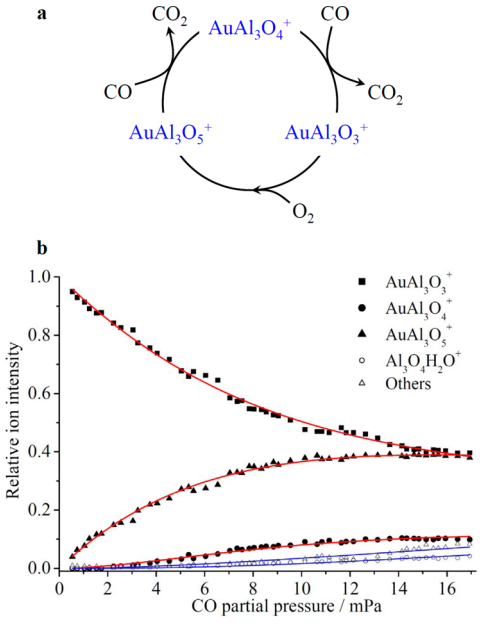


**Figure 2.** Catalytic cycle (a) and the reaction kinetics (b). The variation of ion intensities with respect to the partial pressures of CO in the reactions of $AuAl_3O_3^+$ with gas mixture of CO and $O_2$ is shown in panel b. The ratio of partial pressure of CO to $O_2$ was 1:1, and the reaction time was 1.0 ms. The data points were experimentally measured, and the solid lines were calculated on the basis of rate constants determined from least-squares fitting.

The reaction kinetics for the identified catalysis in Figure 2a was investigated, and the result is shown in Figure 2b. In the reactions of $AuAl_3O_3^+$ cluster ions with the gas mixture of CO and $O_2$, as the partial pressures of reactant molecules increased, the relative ion intensity of $AuAl_3O_3^+$ decreased and those of $AuAl_3O_{4,5}^+$ increased gradually. Note that the formations of product ions that correspond to catalyst deactivation can be negligible (<4%) at low CO partial pressures (<10 mPa, Figure 2b). It turns out that the relative ion intensities of $AuAl_3O_{3-5}^+$ can be well fitted by assuming a pseudo-first-order reaction mechanism in each of the elementary steps. The rate constants determined from the catalytic reactions (the last column of Table 1) match those from the elementary reactions (the second column of Table 1) within a factor of 2. In the catalytic reactions, the heat of formation of the net reaction (CO burning, reaction 5) can excite the intracluster vibrations. As a result, the effective temperature of the clusters[24] during the catalysis is higher than that before the catalysis, which can be used to interpret the differences in the rate constants from elementary and catalytic reactions (Figure S6 in the Supporting Information).

**3.2. Computational Results.** Quantum chemistry calculations with density functional theory have been employed to study the mechanism of CO oxidation catalyzed by the $AuAl_3O_{3-5}^+$ clusters. The lowest energy structure of the $AuAl_3O_5^+$ cluster (Figure S22 in the Supporting Information) has a doublet spin multiplicity, and the spin density is distributed on Au and two adjacent O atoms (Figure 3a). In the reaction of $AuAl_3O_5^+$ with CO, the CO molecule can be adsorbed on both Au and Al atoms (Figures S12 and S13 in the Supporting Information). The Al-site adsorption results in formation of the association product $AuAl_3O_5CO^+$ (reaction 2b), while the Au-site adsorption proceeds to CO oxidation (reaction 2a), during which all of the transition states (TS1−TS3 in Figure 3b) are much lower in energy than the separated reactants ($AuAl_3O_5^+$ + CO). After oxidation of CO by the $AuAl_3O_5^+$ cluster, in which the Au atom is bonded with two oxygen atoms, the Au is bonded with one Al atom in $AuAl_3O_4^+$. The conversion of gold−oxygen to gold−metal bonds during the chemical reactions has been recently reported for a few elementary cluster reactions,[25] and this study serves as a first example to demonstrate that such a conversion is involved in catalytic cluster reactions.


dx.doi.org/10.1021/ja508547z | J. Am. Chem. Soc. 2014, 136, 14307−14313

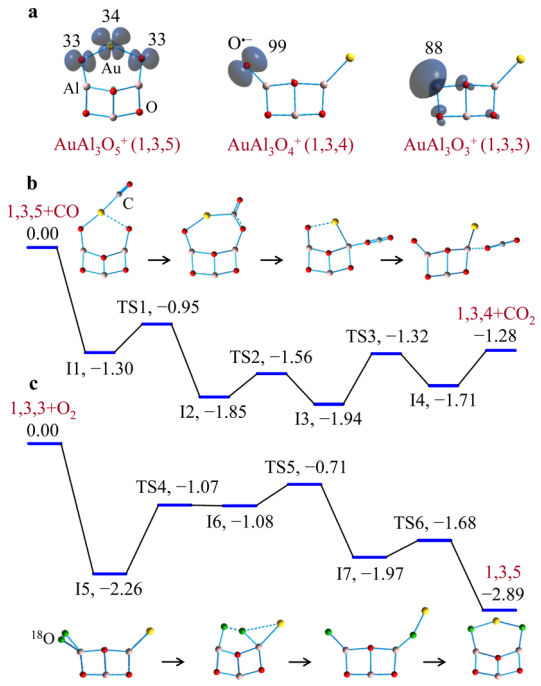


**Figure 3.** Structures and reaction mechanisms. Panel a shows the lowest energy structures of $AuAl_3O_{3-5}^+$. The spin density distributions and percentages on individual atoms are shown. Panels b and c plot potential energy profiles for reactions 2a and 4, respectively. The relative energies of intermediates (I1−I7), transition states (TS1−TS6), and products are in units of eV. The structures of I1−I7 are shown. See Figures S12−S16 in the Supporting Information for detailed information on cluster structures and mechanisms of reactions 3a and 4

After delivering one O atom to CO, the $AuAl_3O_5^+$ cluster is converted to $AuAl_3O_4^+$ (Figure 3a and Figure S21 in the Supporting Information), in which the spin density of about 100% is distributed on a single O atom. Such an O atom is termed as an oxygen-centered radical or atomic oxygen radical anion ($O^{\bullet-}$). The previous investigations have demonstrated that the $O^{\bullet-}$ radical is very oxidative in the reactions with many small molecules including CO.[6d,10c,26] Due to the presence of the $O^{\bullet-}$ center in $AuAl_3O_4^+$, reaction 3a is highly exothermic and facile (Figure S14 in the Supporting Information). This is also in agreement with the experimental observation of a very fast oxidation of CO by $AuAl_3O_4^+$ (Table 1). It is noteworthy that the $^{16}O/^{18}O$ exchange process observed for $AuAl_3O_4^+$ (Figure 1h) rather than for $AuAl_3O_3^+$ (Figure 1g) and $AuAl_3O_5^+$ (Figure 1i) is also due to the presence of the $O^{\bullet-}$ radical in this particular cluster (Figure S19 in the Supporting Information).

After the consecutive oxidation of two CO molecules, the $AuAl_3O_5^+$ cluster is converted to $AuAl_3O_3^+$ (Figure 3a and Figure S20 in the Supporting Information), the spin density of which is mainly distributed on an Al atom that can adsorb an $O_2$ molecule (see I5 in Figure 3c) with a binding energy greater than 2 eV. The $O_2$ in the intermediate I5 is significantly activated to superoxide radical $O_2^{\bullet-}$ (O−O bond length of 140 pm versus 122 pm for free $O_2$; Figure S16 in the Supporting Information). Further reduction of $O_2^{\bullet-}$ (I5 → TS4 → I6 → TS5 → I7) can be achieved by releasing two paired electrons stored in the Au−Al chemical bond. The most stable structure of $AuAl_3O_5^+$ is lower in energy than I5 by 0.63 eV, and the energy of the crucial transition state (TS5) for O−O bond breaking is lower than that of the separated reactants ($AuAl_3O_3^+$ and $O_2$) by 0.71 eV; thus, regeneration of $AuAl_3O_5^+$ with the lowest energy structure from the gas-phase reaction (4) is both thermodynamically and kinetically favorable. Further computational studies indicate that, in the reaction of $AuAl_3{}^{16}O_3^+$ with $^{18}O_2$, the $^{16}O/^{18}O$ isotopic scrambling can take place for any of the three $^{16}O$ atoms (Figure S16). This gives a good interpretation of the generation of the fully $^{18}O$ substituted clusters $AuAl_3{}^{18}O_3^+$, $AuAl_3{}^{18}O_4^+$, and $AuAl_3{}^{18}O_5^+$ in Figure 1j. It can be seen that the quantum chemistry calculations support and interpret the experimental observations very well.

## 4. DISCUSSION

**4.1. Comparison with Reported Gas-Phase Cluster Catalysis.** The catalytic CO oxidation mediated with gas-phase species has been extensively studied.[6c,d,10,27] None of the reported NM-free species are able to catalyze CO oxidation by $O_2$, while many of them can catalyze CO oxidation by $N_2O$, an oxidant that tends to supply an oxygen atom (bond enthalpies of $N_2-O$ = 1.73 eV and O−O = 5.16 eV). For example, the $Al_2O_2^+/Al_2O_3^+$, $VO_2/VO_3$, $AlVO_3^+/AlVO_4^+$, and $AlYO_2^+/AlYO_3^+$ cluster couples[28] have been reported to be able to catalyze the reaction CO + $N_2O$ → $CO_2$ + $N_2$ rather than 2CO + $O_2$ → 2$CO_2$. The oxidation of CO by $O_2$ can be catalyzed by NM species, but each of the reported catalytic systems has at least two NM atoms, such as $Au_{2,6}^-$, $Ag_{7,9,11}^-$, $Au_3(CO)_{2-5}$, $Pt_{3-6}^-$, and $Pd_6O_4^+$.[10a,29]

In order to understand the catalytic importance of single NM atoms in the CO oxidation, bimetallic oxide clusters, including $AuTi_xO_y^{\pm}$ and $AuFe_xO_y^-$, have been recently generated and interacted with CO.[25b,c,30] The promotion effect of gold in the elementary CO oxidation has been demonstrated.[25b,c] However, attempts to identify the catalytic CO oxidation by $O_2$ were not successful[25b] because the investigated cluster products generated in the elementary CO oxidation cannot further react with $O_2$ to close a catalytic cycle. For the first time, this study reports that the single NM atoms (Au) supported on appropriate NM-free clusters ($Al_3O_{3-5}$) can really be catalytic in the CO oxidation by $O_2$. The identified gas-phase catalysis (Figure 2a) not only parallels similar behaviors of bulk oxide supported gold catalysts but also interprets how and why a supported NM atom can be catalytic at strictly a molecular level (see the discussion below).

**4.2. Comparison with Condensed-Phase Catalysis.** The mechanisms of CO oxidation catalyzed by oxide-supported gold catalysts such as Au/$TiO_2$, Au/$Al_2O_3$, and so on have been extensively studied.[7,8,31] The catalytic importance of the perimeter of Au particles as well as the oxide supports has been recognized. A very recent experiment identified dual catalytic sites on the Au/$TiO_2$ catalyst: delivery and oxidation of CO take place from both oxide ($TiO_2$) and gold sites.[7b] The model catalysis of this study (Figure 2a) parallels the above mechanism well because the first CO molecule is captured and delivered for oxidation by Au (Figure 3b) while the second one is captured and oxidized directly by the $O^{\bullet-}$ radical on the "oxide support", the $Al_3O_4$ cluster moiety (Figure S14 in the Supporting Information). It is interesting that the first oxidation and the second oxidation of CO on the small atomic clusters $AuAl_3O_{4,5}^+$ have different mechanisms. The conversion of the $AuAl_3{}^{16}O_3^+$ cluster catalyst into $AuAl_3{}^{18}O_3^+$ in the $^{18}O_2$ experiment (Figure 1j) confirms the direct participation of "oxide support" in the catalytic CO oxidation, which was


dx.doi.org/10.1021/ja508547z | J. Am. Chem. Soc. 2014, 136, 14307−14313

proposed in many condensed-phase studies.[7b,c,8,31] It is noteworthy that previous investigations have emphasized the involvement of the reactive oxygen species (ROS) $O_2^{\bullet-}$, $O_2^{2-}$, and $O^{\bullet-}$ in the catalytic CO oxidation on the oxide-supported gold catalysts.[32] Two of the three ROS, superoxide radical $O_2^{\bullet-}$ (I5 in Figure 3c) and atomic oxygen radical $O^{\bullet-}$ ($AuAl_3O_4^+$ in Figure 3a), are present in the gas-phase catalysis of this study.

In addition to the catalytic sites and the presence of the ROS, charge transfer between gold particles and the oxide supports has also been emphasized in the literature.[8,33] Figure 4 indicates

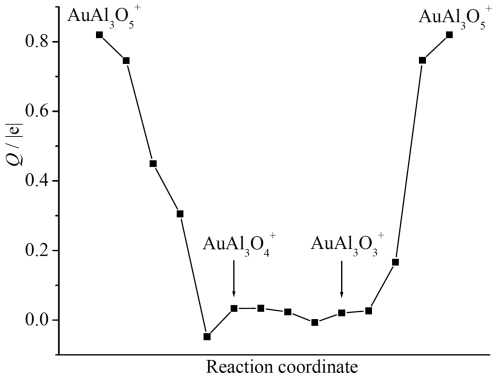


**Figure 4.** Charge cycling on the gold atoms during the catalytic cycle of Figure 2a. The charges on Au atoms of $AuAl_3O_5^+$, I1–I4 (Figure 3b), $AuAl_3O_4^+$, I9′, and I10′ (Figure S14 in the Supporting Information), $AuAl_3O_3^+$, and I5–I7 (Figure 3c) along the reaction coordinate are given on the basis of natural bond orbital analysis.

that, in the cluster catalysis, the gold atom accepts a significant amount of negative charge (−0.87e) during oxidation of the first CO molecule (reaction 2a) and the negative charge is released during reduction of oxygen molecule (reaction 4). It can be concluded that the catalysis of single gold atoms on oxide clusters (Figure 2a) parallels the catalysis of gold particles on bulk oxides well, implying that both systems can have the same physical origin.

**4.3. Catalytic Mechanism and Its Physical Origin.** The identified model catalysis of this study follows a typical redox mechanism, by which CO is oxidized by the oxygen of the catalyst ($AuAl_3O_{4,5}^+$) and the reduced catalyst ($AuAl_3O_3^+$) is oxidized by gas-phase $O_2$. The fundamental scientific problem involved with the redox mechanism is the activation of molecular oxygen: $O_2 \rightarrow O_2^{\bullet-} \rightarrow O_2^{2-} \rightarrow O^{2-} + O^{\bullet-} \rightarrow 2O^{2-}$.[26c,32,34] At least three electrons are required to reduce one $O_2$ molecule into atomic oxygen species ($O_2 + 3e \rightarrow O^{2-} + O^{\bullet-}$). Figure 3b indicates that two electrons that will be used to reduce $O_2$ are stored in the Au–Al chemical bond of $AuAl_3O_4^+$ produced from the oxidation of the first CO molecule ($O^{2-} + CO \rightarrow CO_2 + 2e^-$). One additional electron is released upon oxidation of the second CO through the facile radical process ($O^{\bullet-} + CO \rightarrow CO_2 + e^-$ and Figure S14 in the Supporting Information).

The bonding character of $AuAl_3O_4^+$ (Figure 3a) is unique because this cluster contains both a *reductive* metal–metal (Au–Al) bond and highly *oxidative* $O^{\bullet-}$ radical center. The strong relativistic effect[35] which increases the electron affinity of Au atom by a factor of about 2[35c] leads to a contracted and stabilized Au 6s orbital; thus, gold tends to accept an electron[36] and make polarized and relatively strong chemical bonds with metal atoms. The Au–Al bond energy in $AuAl_3O_4^+$ amounts to 3.41 eV by the DFT calculations. It is noteworthy that a very recent photoelectron spectroscopic study of the $Au_2(AlO)_2$ cluster reported an average calculated Au–Al bond energy of 3.3 eV.[37] In contrast, if the Au atom in the most stable structure of $AuAl_3O_4^+$ is replaced by an Ag atom, the Ag–Al bond energy is only 2.92 eV and this Ag–Al bond will be oxidized by the nearby $O^{\bullet-}$ radical to generate a more stable structure of $AgAl_3O_4^+$ with an Ag–O bond (Figure S23 in the Supporting Information). In the experiment (Figure S11 in the Supporting Information), the $AgAl_3O_4^+$ cluster adsorbs rather than oxidizes CO. As a result, the catalytic process of Figure 2a does not take place for the silver counterpart.

The Au–Al bond is strong enough to survive in the $AuAl_3O_4^+$ cluster with four O atoms (Figure 3a and Figure S21 in the Supporting Information). However, when the system ($AuAl_3O_5^+$) has an additional O atom, the Au–Al bond tends to cleave (I5 → I6 → I7 → 1,3,5 in Figure 3c) to release valence electrons to reduce oxygen and to break the O–O bond, so that the CO oxidation can be cycled. It can be concluded that the gold–metal (Au–Al) bond making and breaking drives the single Au atom catalysis that has a physical origin in the relativistic effect.

## 5. CONCLUSION

The catalytic oxidation of carbon monoxide by molecular oxygen mediated with atomic cluster supported gold species $AuAl_3O_{3-5}^+$ has been identified and characterized by mass spectrometry and quantum chemistry calculations. To the best of our knowledge, this is the first example of catalytic CO oxidation by $O_2$ on gas-phase cluster catalysts with single noble-metal atoms. The electron cycling primarily through making and breaking a gold–aluminum chemical bond drives the catalysis. The formation of a reductive gold–aluminum bond in the presence of a highly oxidative atomic oxygen radical is essential for the catalysis, and this mechanism has a physical origin in the relativistic effect. The identified gas-phase catalysis parallels and provides insights into the heterogeneous gold catalysis in terms of active sites, support effects (direct participation and supply of reactive oxygen species), and the interaction (charge transfer) between the gold and the supports. This work has also demonstrated that single-atom catalysis can be interpreted at strictly a molecular level on the basis of the cluster research. Mechanisms of important single-atom catalysis with other noble-metal atoms, including Pt, Rh, and so on, will be studied with the cluster approach in the future.

## ■ ASSOCIATED CONTENT

### Supporting Information

Figures giving additional mass spectra, data analysis, and DFT calculated cluster structures and reaction mechanisms and a table giving related bond dissociation energies by experiments and DFT calculations. This material is available free of charge via the Internet at http://pubs.acs.org.

## ■ AUTHOR INFORMATION

### Corresponding Authors

*E-mail for X.-N.L.: lxn@iccas.ac.cn.
*E-mail for S.-G.H.: shengguihe@iccas.ac.cn.

### Notes

The authors declare no competing financial interest.

## ■ ACKNOWLEDGMENTS

This work was supported by the Major Research Plan of China (Nos. 2013CB834603 and 2011CB932302), the National Natural Science Foundation of China (Nos. 21325314 and 21303215), and the Institute of Chemistry, Chinese Academy of Sciences (No. CMS-PY-201306).

## ■ REFERENCES

(1) (a) Yang, X. F.; Wang, A.; Qiao, B.; Li, J.; Liu, J.; Zhang, T. *Acc. Chem. Res.* **2013**, *46*, 1740−1748. (b) Flytzani-Stephanopoulos, M. *Acc. Chem. Res.* **2014**, *47*, 783−792.

(2) (a) Qiao, B.; Wang, A.; Yang, X.; Allard, L. F.; Jiang, Z.; Cui, Y.; Liu, J.; Li, J.; Zhang, T. *Nat. Chem.* **2011**, *3*, 634−641. (b) Moses-DeBusk, M.; Yoon, M.; Allard, L. F.; Mullins, D. R.; Wu, Z.; Yang, X.; Veith, G.; Stocks, G. M.; Narula, C. K. *J. Am. Chem. Soc.* **2013**, *135*, 12634−12645.

(3) (a) Fu, Q.; Saltsburg, H.; Flytzani-Stephanopoulos, M. *Science* **2003**, *301*, 935−938. (b) Zhai, Y.; Pierre, D.; Si, R.; Deng, W.; Ferrin, P.; Nilekar, A. U.; Peng, G.; Herron, J. A.; Bell, D. C.; Saltsburg, H.; Mavrikakis, M.; Flytzani-Stephanopoulos, M. *Science* **2010**, *329*, 1633−1636.

(4) (a) Zhang, X.; Shi, H.; Xu, B. Q. *Angew. Chem., Int. Ed.* **2005**, *44*, 7132−7135. (b) Kyriakou, G.; Boucher, M. B.; Jewell, A. D.; Lewis, E. A.; Lawton, T. J.; Baber, A. E.; Tierney, H. L.; Flytzani-Stephanopoulos, M.; Sykes, E. C. H. *Science* **2012**, *335*, 1209−1212.

(5) Chang, T. Y.; Tanaka, Y.; Ishikawa, R.; Toyoura, K.; Matsunaga, K.; Ikuhara, Y.; Shibata, N. *Nano Lett.* **2014**, *14*, 134−138.

(6) (a) Muetterties, E. L. *Science* **1977**, *196*, 839−848. (b) Armentrout, P. B. *Annu. Rev. Phys. Chem.* **2001**, *52*, 423−461. (c) Böhme, D. K.; Schwarz, H. *Angew. Chem., Int. Ed.* **2005**, *44*, 2336−2354. (d) Castleman, A. W., Jr. *Catal. Lett.* **2011**, *141*, 1243−1253.

(7) (a) Valden, M.; Lai, X.; Goodman, D. W. *Science* **1998**, *281*, 1647−1650. (b) Green, I. X.; Tang, W.; Neurock, M.; Yates, J. T., Jr. *Science* **2011**, *333*, 736−739. (c) Akita, T.; Kohyama, M.; Haruta, M. *Acc. Chem. Res.* **2013**, *46*, 1773−1782.

(8) Yoon, B.; Häkkinen, H.; Landman, U.; Wörz, A. S.; Antonietti, J. M.; Abbet, S.; Judai, K.; Heiz, U. *Science* **2005**, *307*, 403−407.

(9) Lee, S.; Fan, C.; Wu, T.; Anderson, S. L. *J. Am. Chem. Soc.* **2004**, *126*, 5682−5683.

(10) (a) Socaciu, L. D.; Hagen, J.; Bernhardt, T. M.; Wöste, L.; Heiz, U.; Häkkinen, H.; Landman, U. *J. Am. Chem. Soc.* **2003**, *125*, 10437−10445. (b) Kimble, M. L.; Moore, N. A.; Johnson, G. E.; Castleman, A. W., Jr.; Bürgel, C.; Mitrić, R.; Bonačić-Koutecký, V. *J. Chem. Phys.* **2006**, *125*, 204311. (c) Liu, Q.-Y.; He, S.-G. *Chem. J. Chin. Univ.* **2014**, *35*, 665−688.

(11) Lu, J.; Aydin, C.; Browning, N. D.; Gates, B. C. *Angew. Chem., Int. Ed.* **2012**, *51*, 5842−5846.

(12) (a) Yuan, Z.; Li, Z.-Y.; Zhou, Z.-X.; Liu, Q.-Y.; Zhao, Y.-X.; He, S.-G. *J. Phys. Chem. C* **2014**, *118*, 14967−14976. (b) Zhao, Y.-X.; Li, Z.-Y.; Yuan, Z.; Li, X.-N; He, S.-G. *Angew. Chem., Int. Ed.* **2014**, *53*, 9482−9486.

(13) Wu, X.-N.; Xu, B.; Meng, J.-H.; He, S.-G. *Int. J. Mass Spectrom.* **2012**, *310*, 57−64.

(14) Yuan, Z.; Zhao, Y.-X.; Li, X.-N.; He, S.-G. *Int. J. Mass Spectrom.* **2013**, *354*−*355*, 105−112.

(15) Kummerlöwe, G.; Beyer, M. K. *Int. J. Mass Spectrom.* **2005**, *244*, 84−90.

(16) Frisch, M. J.; Trucks, G. W.; Schlegel, H. B.; Scuseria, G. E.; Robb, M. A.; Cheeseman, J. R.; Scalmani, G.; Barone, V.; Mennucci, B.; Petersson, G. A.; Nakatsuji, H.; Caricato, M.; Li, X.; Hratchian, H. P.; Izmaylov, A. F.; Bloino, J.; Zheng, G.; Sonnenberg, J. L.; Hada, M.; Ehara, M.; Toyota, K.; Fukuda, R.; Hasegawa, J.; Ishida, M.; Nakajima, T.; Honda, Y.; Kitao, O.; Nakai, H.; Vreven, T.; Montgomery, J. A., Jr.; Peralta, J. E.; Ogliaro, F.; Bearpark, M.; Heyd, J. J.; Brothers, E.; Kudin, K. N.; Staroverov, V. N.; Kobayashi, R.; Normand, J.; Raghavachari, K.; Rendell, A.; Burant, J. C.; Iyengar, S. S.; Tomasi, J.; Cossi, M.; Rega, N.; Millam, J. M.; Klene, M.; Knox, J. E.; Cross, J. B.; Bakken, V.; Adamo, C.; Jaramillo, J.; Gomperts, R.; Stratmann, R. E.; Yazyev, O.; Austin, A. J.; Cammi, R.; Pomelli, C.; Ochterski, J. W.; Martin, R. L.; Morokuma, K.; Zakrzewski, V. G.; Voth, G. A.; Salvador, P.; Dannenberg, J. J.; Dapprich, S.; Daniels, A. D.; Farkas, O.; Foresman, J. B.; Ortiz, J. V.; Cioslowski, J.; Fox, D. J. *Gaussian 09, Revision A.1*; Gaussian, Inc., Wallingford, CT, 2009.

(17) Schäfer, A.; Huber, C.; Ahlrichs, R. *J. Chem. Phys.* **1994**, *100*, 5829−5835.

(18) Dolg, M.; Stoll, H.; Preuss, H. *J. Chem. Phys.* **1989**, *90*, 1730−1734.

(19) Tao, J.; Perdew, J. P.; Staroverov, V. N.; Scuseria, G. E. *Phys. Rev. Lett.* **2003**, *91*, 146401.

(20) Ding, X.-L.; Li, Z.-Y.; Meng, J.-H.; Zhao, Y.-X.; He, S.-G. *J. Chem. Phys.* **2012**, *137*, 214311.

(21) Berente, I.; Náray-Szabó, G. *J. Phys. Chem. A* **2006**, *110*, 772−778.

(22) Glendening, E. D.; Reed, A. E.; Carpenter, J. E.; Weinhold, F. *NBO 3.1*; Theoretical Chemistry Institute, University of Wisconsin, Madison, WI, 1996.

(23) Balaj, O. P.; Balteanu, I.; Roβteuscher, T. T. J.; Beyer, M. K.; Bondybey, V. E. *Angew. Chem., Int. Ed.* **2004**, *43*, 6519−6522.

(24) Bondybey, V. E.; Beyer, M. K. *J. Phys. Chem. A* **2001**, *105*, 951−960.

(25) (a) Wu, X.-N.; Li, X.-N.; Ding, X.-L.; He, S.-G. *Angew. Chem., Int. Ed.* **2013**, *52*, 2444−2448. (b) Li, X.-N.; Yuan, Z.; He, S.-G. *J. Am. Chem. Soc.* **2014**, *136*, 3617−3623. (c) Yuan, Z.; Li, X.-N.; He, S.-G. *J. Phys. Chem. Lett.* **2014**, *5*, 1585−1590.

(26) (a) Dietl, N.; Schlangen, M.; Schwarz, H. *Angew. Chem., Int. Ed.* **2012**, *51*, 5544−5555. (b) Ding, X.-L.; Wu, X.-N.; Zhao, Y.-X.; He, S.-G. *Acc. Chem. Res.* **2012**, *45*, 382−390. (c) Che, M.; Tench, A. J. *Adv. Catal.* **1982**, *31*, 77−133.

(27) (a) Schlangen, M.; Schwarz, H. *Catal. Lett.* **2012**, *142*, 1265−1278. (b) Yin, S.; Bernstein, E. R. *Int. J. Mass Spectrom.* **2012**, *321*−*322*, 49−65. (c) Lang, S. M.; Bernhardt, T. M. *Phys. Chem. Chem. Phys.* **2012**, *14*, 9255−9269. (d) Zhao, Y.-X.; Wu, X.-N.; Ma, J.-B.; He, S.-G.; Ding, X.-L. *Phys. Chem. Chem. Phys.* **2011**, *13*, 1925−1938. (e) Johnson, G. E.; Mitrić, R.; Bonačić-Koutecký, V.; Castleman, A. W., Jr. *Chem. Phys. Lett.* **2009**, *475*, 1−9. (f) O'Hair, R. A. J.; Khairallah, G. N. *J. Cluster Sci.* **2014**, *15*, 331−363.

(28) (a) Johnson, G. E.; Tyo, E. C.; Castleman, A. W., Jr. *J. Phys. Chem. A* **2008**, *112*, 4732−4735. (b) Wang, Z. C.; Yin, S.; Bernstein, E. R. *Phys. Chem. Chem. Phys.* **2013**, *15*, 10429−10434. (c) Wang, Z. C.; Dietl, N.; Kretschmer, R.; Weiske, T.; Schlangen, M.; Schwarz, H. *Angew. Chem., Int. Ed.* **2011**, *50*, 12351−12354. (d) Ma, J.-B.; Wang, Z. C.; Schlangen, M.; He, S.-G.; Schwarz, H. *Angew. Chem., Int. Ed.* **2013**, *52*, 1226−1230.

(29) (a) Wallace, W. T.; Whetten, R. L. *J. Am. Chem. Soc.* **2002**, *124*, 7499−7505. (b) Socaciu, L. D.; Hagen, J.; Le Roux, J.; Popolan, D.; Bernhardt, T. M.; Wöste, L.; Vajda, S. *J. Chem. Phys.* **2004**, *120*, 2078−2081. (c) Xie, Y.; Dong, F.; Bernstein, E. R. *Catal. Today* **2011**, *177*, 64−71. (d) Shi, Y.; Ervin, K. M. *J. Chem. Phys.* **1998**, *108*, 1757−1760. (e) Lang, S.; Fleischer, M. I.; Bernhardt, T. M.; Barnett, R. N.; Landman, U. *J. Am. Chem. Soc.* **2012**, *134*, 20654−20659.

(30) Himeno, H.; Miyajima, K.; Yasuike, T.; Mafuné, F. *J. Phys. Chem. A* **2011**, *115*, 11479−11485.

(31) (a) Min, B. K.; Friend, C. M. *Chem. Rev.* **2007**, *107*, 2709−2724. (b) Freund, H. J.; Meijer, G.; Scheffler, M.; Schlogl, R.; Wolf, M. *Angew. Chem., Int. Ed.* **2011**, *50*, 10064−10094. (c) Royer, S.; Duprez, D. *ChemCatChem* **2011**, *3*, 24−65.

(32) (a) Widmann, D.; Liu, Y.; Schüth, F.; Behm, R. J. *J. Catal.* **2010**, *276*, 292−305. (b) Widmann, D.; Behm, R. J. *Angew. Chem., Int. Ed.* **2011**, *50*, 10241−10245. (c) Carrettin, S.; Concepción, P.; Corma, A.; Nieto, J. M. L.; Puntes, V. F. *Angew. Chem., Int. Ed.* **2004**, *43*, 2538−2540. (d) Guzman, J.; Carrettin, S.; Fierro-Gonzalez, J. C.; Hao, Y. L.; Gates, B. C.; Corma, A. *Angew. Chem., Int. Ed.* **2005**, *44*, 4778−4781. (e) Ma, J.-B.; Xu, B.; Meng, J.-H.; Wu, X.-N.; Ding, X.-L.; Li, X.-N.; He, S.-G. *J. Am. Chem. Soc.* **2013**, *135*, 2991−2998.

(33) (a) Wang, Y.-G.; Yoon, Y.; Glezakou, V. A.; Li, J.; Rousseau, R. *J. Am. Chem. Soc.* **2013**, *135*, 10673−10683. (b) Manzoli, M.; Boccuzzi,

F.; Chiorino, A.; Vindigni, F.; Deng, W.; Flytzani-Stephanopoulos, M. *J. Catal.* **2007**, *245*, 308−315.
(34) (a) Woodham, A. P.; Meijer, G.; Fielicke, A. *Angew. Chem., Int. Ed.* **2012**, *51*, 4444−4447. (b) Pal, R.; Wang, L.-M.; Pei, Y.; Wang, L.-S.; Zheng, X. C. *J. Am. Chem. Soc.* **2012**, *134*, 9438−9445.
(35) (a) Pyykkö, P.; Desclaux, J. P. *Acc. Chem. Res.* **1979**, *12*, 276−281. (b) Schwarz, H. *Angew. Chem., Int. Ed.* **2003**, *42*, 4442−4454. (c) Pyykkö, P. *Angew. Chem., Int. Ed.* **2004**, *43*, 4412−4456. (d) Gorin, D. J.; Toste, F. D. *Nature* **2007**, *446*, 395−403. (e) Wang, L.-S. *Phys. Chem. Chem. Phys.* **2010**, *12*, 8694−8705.
(36) Jansen, M. *Chem. Soc. Rev.* **2008**, *37*, 1826−1835.
(37) Lopez, G. V.; Jian, T.; Li, W.-L.; Wang, L.-S. *J. Phys. Chem. A* **2014**, *118*, 5204−5211.